University of Iowa

Iowa Research Online

Summer 2014

Development and application of a simple terrestrial laser scanner

Sean Plenner
University of Iowa

Follow this and additional works at: https://ir.uiowa.edu/etd

Part of the Civil and Environmental Engineering Commons

Recommended Citation
Plenner, Sean. "Development and application of a simple terrestrial laser scanner." MS (Master of Science) thesis, University of Iowa, 2014.
https://doi.org/10.17077/etd.qa5jvjtg

www.manaraa.com

DEVELOPMENT AND APPLICATION OF A SIMPLE

TERRESTRIAL LASER SCANNER

by

Sean Plenner

A thesis submitted in partial fulfillment
of the requirements for the Master of
Science degree in Civil and Environmental Engineering
in the Graduate College of
The University of Iowa

August 2014

Thesis Supervisor: Professor William E. Eichinger

Graduate College
The University of Iowa
Iowa City, IA

CERTIFICATE OF APPROVAL

_____

MASTER'S THESIS

_____

This is to certify that the Master's thesis of

Sean Plenner

has been approved by the Examining Committee
for the thesis requirement for the Master of Science
degree in Civil and Environmental Engineering at the August 2014 graduation.

Thesis Committee: _____
                            William E. Eichinger, Thesis Supervisor

                            _____
                            Marian Muste

                            _____
                            E. Arthur Bettis

To My Friends and Family

ACKNOWLEDGMENTS

First, I would like to thank Bill for initiating this project and supporting it all the way through. He offered many practical ideas and solutions that made this project possible. From the many long drives to field experiments across the country, Bill has aroused my insatiable curiosity for learning new things outside my area of expertise. I would also like to thank Dan Ceynar for helping brainstorm ideas for this project and help to take it from the conceptual stage into fruition.

TABLE OF CONTENTS

LIST OF TABLES

LIST OF FIGURES

CHAPTER 1. INTRODUCTION

Since the texture of surfaces plays a key role in the shaping of many environmental processes, high resolution measurements are important to study these phenomena. Specifically, 3-D point cloud data is desirable to document river shape and evolution, surface roughness, and erosion-sedimentation processes. In addition, accurate estimation of the amount of flow in a river requires knowledge of the river shape and roughness. Surface roughness describes the micro-variations in surface elevation amongst other contributors and is a major factor influencing erosion (Moreno et al., 2010). High-intensity precipitation is also a major contributor to surface erosion by dislodging particles and transporting them downstream. Also, laboratory experiments of erosional and depositional features are in need of a simple, affordable, and robust system of measuring bed topography at high resolution. This research focuses on the development of a new measurement system that is used to acquire high resolution data relating to hydraulic and fluvial environments.

CHAPTER 2. BACKGROUND

2.1. Available Technology

Physical characteristics of a surface are documented using many different instruments including but not limited to: roller chain, pin meter, stereo-photography, total station, traverse mounted laser scanner, or terrestrial laser scanner (TLS). For the purposes of this research, a total station was not analyzed since it is not automated, has difficulty producing small scale results with acceptable accuracy, and potentially disturbs the surface each time a measurement is made.

Roller chains sets are used to document soil surface roughness by carefully placing them to follow the micro-relief and subsequently measuring the horizontal reach of each chain by a caliper (Fig. 2.1). They are imprecise, time-consuming at measuring micro-relief, and can potentially disturb the surface being measured (Merrill et al., 2001; Gilley & Kottwitz, 1995).

Figure 2.1 Chain set used to measure soil surface roughness (Moreno et al., 2010)

Pin meter (Fig. 2.2) is another laborious instrument that documents micro-relief by manually lowering 50 pins at distances of 20 mm. After lowering the pins, a camera and associated software can be used to record pin positions as micro-topographic readings. The pin meter would be shifted 20 mm after each reading to get a grid of 2500 readings/m^2 with resolution of 20 x 20 mm (Moreno et al., 2010).

Figure 2.2 Pin meter used to measure soil topography (Moran)

Stereo-photography combines images from two cameras separated by a known distance to yield 3-d coordinates of the imaged and combined surface (Fig. 2.3). Common tie-points are identified on each image to allow the transformation software to be applied correctly. This inexpensive technique is limited by extensive post-processing to yield accurate results. It has been used to measure soil erosion and rill development (Rieke-Zapp et al., 2001; Rieke-Zapp et al., 2005). Digital photogrammetry has also been applied at close range to acquire finely resolved (6 x 6 mm) XYZ positional information of an eroding soil bed (Nouwakpo et al., 2010).
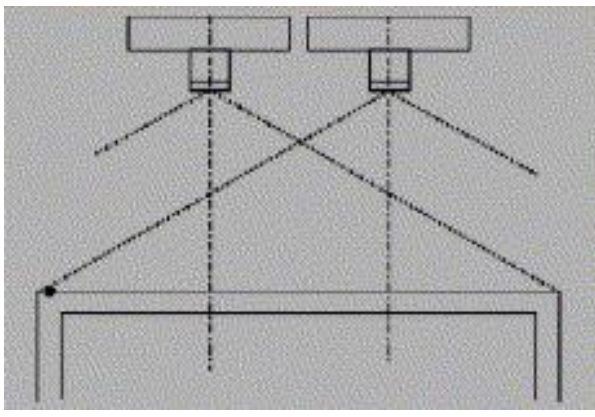
Figure 2.3 Stereo-photography (Jester & Klik, 2005)

Track mounted laser scanners measure surface elevation by optical triangulation (Jester & Klik, 2005). Since they are mounted on a movable carriage (Fig. 2.4), they automatically traverse and survey a surface quickly. Since a camera is used to digitize the laser profile, they often lack filters to block sunlight and therefore must scan at night or in a laboratory. They also lack the ability to scan steep slopes.
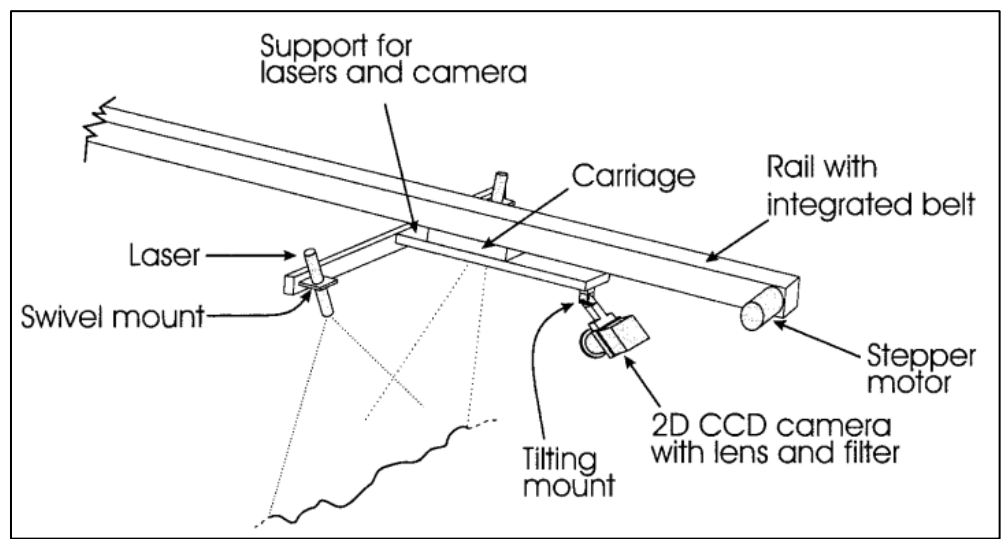
Figure 2.4 Laser and camera assembly mounted on a moving traverse (Darboux & Huang, 2003)

Because of time, cost, and slope issues, the above measurement systems are not suitable for a wide range of experimental desires. The most efficient instrument used to profile a surface is a terrestrial laser scanner (TLS). TLSs combine a form of distance measurement with a positioning system. Most commercial laser scanners make use of a spinning mirror to rapidly determine position. The three main methods of determining distance include triangulation, interferometry, and time-of-flight (Zogg, 2008); each method has specific uses in diverse fields from reverse engineering to mountain surveying.

Figure 2.5 Commercial terrestrial laser scanner that provides accurate 3-D model of a bridge structure (RUDI, 2014)

2.2. Methods of Distance Measurement

Precise distance measurement is acquired using optical triangulation with known geometrical relationships. Instruments that employ this principle are typically short-range

and used more for industrial applications and reverse engineering because they can achieve micrometer accuracy (Heritage & Large, 2009).

The interferometry method, also known as the phase difference method, acquires distance by interfering electromagnetic waves and measuring the interference patterns (Zogg, 2008). Instruments which employ interferometry are typically medium range (< 100 m) and accurate to a few millimeters (Heritage & Large, 2009).

The most popular distance measurement method in the laser scanning community is time-of-flight. The time-of-flight principle, also known as LiDAR (Light Detection and Ranging), acquires distance by sending a pulsed laser beam to a target and collecting the reflected signal in a lens that focuses the beam onto a photodiode. Since the speed of light in a medium is constant, the difference in time the signal sent out and reflected back is used to determine distance. Instruments that use time-of-flight principles can be long or medium range and are typically accurate to a few millimeters.

2.3. Applications and Issues

TLSs have been used to investigate volcanic rock slopes (Nguyen et al., 2011) and develop parameters to classify hazardous areas. Rates of streambank retreat (SBR) are important to be able to predict when/if a structure becomes instable and in need of restoration. SBR has been quantified using a TLS to demonstrate the benefits over manual total station data (Resop & Hession, 2010). TLSs have been used to measure gravel size distributions and their associated errors (Hodge, Brasington, & Richards, 2009). TLSs have also been used to measure surface roughness and grain size distributions of a point bar (Entwistle & Fuller, 2009). Currently, a major disadvantage of using commercial TLSs in fluvial environments is that they cannot measure through deep

water (Day, 2012); however, recent research (Smith et al., 2012) has shown that TLSs have been used to document gravel bed surfaces under 0.2 m of water with < 5 mm mean error. Some non-environmental applications using TLSs include bridge inspection (Meral, 2011), underground utility cavern monitoring (Zogg, 2008), damage detection inside incinerators (Zogg, 2008), and analysis of tunnel deformation (Gosliga et al., 2006).

There are many TLS instruments that have similar components; however, each has differing characteristics; optimal ranges, point-to-point resolution, field-of-view, measurement frequency, scanning speed, customizability, cost, etc. The most popular TLS manufacturers include Leica, Zoller+Frohlich, Riegl, Trimble, Faro, and Optech. Some commercial TLSs can acquire up to a million points per second. In addition to 3-dimensional position information, some scanners return reflection intensity and surface color when coupled with a camera (Heritage & Large, 2009); others even include multiple returns for use in documenting vegetation. The price of each system depends on many factors with the least expensive being $59,000 and typical price of $120,000 (including software) from the manufacturers listed above.

CHAPTER 3. INSTRUMENT DEVELOPMENT

After reviewing the available technology, it became evident that a simple, inexpensive, and customizable scanner was required for the diverse aspects of hydraulics and hydrology, including both lab and field experiments. Specific areas of measurement that would benefit from such a scanner include surface processes related to erosion and sedimentation. Since erosion related processes have characteristic lengths in the scale of millimeters (Jester & Klik, 2005), an instrument accurate to millimeters was required.

3.1. Distance Measurement

Since the goal of this project was to develop a robust TLS, limited time and measurement accuracy impinged on building a LiDAR from scratch. Therefore, two different categories of distance measurement (both time-of-flight) were investigated: single point and scanning. The bulk of distance measurement sensors were built to meet the demands of industrial applications such as monitoring cranes, determining bridge clearances, traffic classification, collision avoidance, in-flight refueling, etc. The main problems that arise when utilizing industrial sensors for environmental applications include: inhomogeneous surfaces, sloping surfaces, and beam divergence (Fig. 3.1).
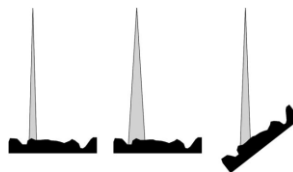
Figure 3.1 Inhomogeneous surfaces

As illustrated in Fig. 3.1, natural surfaces are inhomogeneous due to the roughness or micro-topography that develops from weathering processes of rain drop impact, wind, or decay. Since distance is computed by averaging over the returns generated from the laser beam, inhomogeneous surfaces may result in range inaccuracies, which is known as 'the mixed-edge effect'; therefore, the smallest effective beam divergence is an operational requirement. Likewise, ambiguity increases over sloping surfaces.

Several single-point and one scanning distance measurement system were selected as a possible fit for the applications described above, including: Dimetix DLS-B, Acuity AR1000, and Sick LMS291. The DLS-B15 and AR1000 are laser rangefinders (LRs) with similar specifications (Table 3.1); however, the AR1000 was selected as the optimum LR for environmental applications because it has a smaller beam divergence. The LMS291 was rejected for this project since the accuracy was an order of magnitude lower than desired.

Table 3.1 Comparison of Distance Measurement Systems

Company, Product	Accuracy	Range (nat. surfaces)	Beam Divergence	Frequency	Laser type	Price
Dimetix, DLS-B15	± 1.5 mm	0.05-65 m	8 mm	6, 20 Hz	Class 2	$1795
Acuity, AR1000	± 3 mm	0.1-30 m	5.1 mm	1, 6, 50 Hz	650 nm	$2000
SICK, LMS291	± 35 mm	0-80 m	15 cm	75 Hz	905 nm	$6000

3.2. Position Measurement

Spatially variable environmental processes such as streambank erosion cannot accurately be measured by a single point; a positioning system coupled with a method of measuring erosion (changing distance with time) is needed to relate the process and form. A Directed Perception pan-tilt unit (PTU-D48) was selected as the positioning system

because it is rugged, weatherized, and easy to program. Selected specifications are shown in table 3.2.

Table 3.2 Specifications of Positioning System

		Tilt			Pan		
Company	Product	Range	Res	Max. Speed	Range	Res	Max. Speed
Directed Perception	PTU-D48	+30° to -90°	0.003°	50°/sec	±168°	0.006°	100°/sec

3.3. Mounting and Stability

The LR is fixed to the PTU using a machined ½" aluminum plate. The PTU is mounted to another ½" aluminum plate with a tribrach connector fastened to the underside. The tribrach is connected to an aluminum pipe cap that screws onto the Campbell Scientific CM6 tripod. The CM6 tripod was chosen over a standard surveying tripod because it has a high vantage point (2m tall) and can be staked into the ground for added stability. Before the tribrach was implemented, a corner leveler was used to level the tripod; this was often inaccurate and presented problems when comparing two scans of the same area at different times. All power regulators and cabling are housed in a waterproof aluminum enclosure (Fig. 3.2). The terrestrial laser scanning instrument was named Surface Examining Instrument (SExI). Figure 3.2 shows the entire SExI system with components labeled.
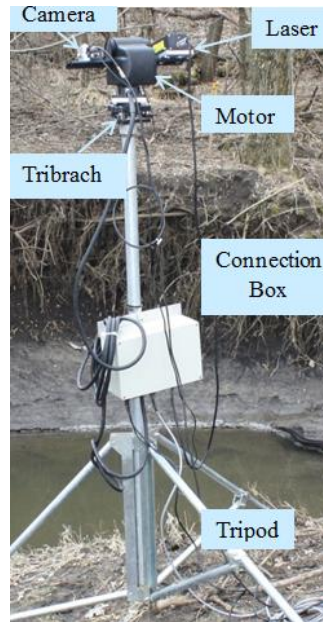
Figure 3.2 Labeled Instrument Setup

3.4. Data Acquisition

After the laser scanner is properly leveled and initialized, an in-house data acquisition program (DAP) written in Pascal automatically controls the movement based on the inputs. Input parameters include initial/final elevation (θ_i, θ_f) and azimuth (Φ_i, Φ_f) angles (in °) and their associated step sizes (in °/step). All input parameter angles are obtained using a 'survey mode' in the DAP that allows the operator to manually point and query position and distance information. A co-axially mounted camera allows the operator to quickly determine the limits of the desired scan area. Two automated modes of scanning have been programmed into the DAP; slow and fast, which acquire data at ~1.8 Hz and ~9 Hz over the entire scan time, respectively. While the fast mode might seem particularly fast compared to the slow mode, it is still ~3 orders of magnitude slower than expensive commercial TLSs that employ a spinning mirror. Slow mode, also

known as 'stare and step', moves by a single step size, queries distance, and moves another single step size, etc. In fast mode, tilt speed is determined by the step size desired while the laser remains at 10 Hz; smaller step size is slower but yields higher resolution. For fast mode, data (azimuth, elevation, and distance) are recorded as the PTU moves from $\theta_{initial}$ to θ_{final}; then the PTU moves at max speed back to $\theta_{initial}$ and shifts one azimuth step. This cycle repeats until Φ_{final} and θ_{final} are reached; then the temporary values are written to a text file. Due to the temporary values only being written to a text file upon scan completion, any power interruptions will render all data lost. The PTU moves at max speed from θ_{final} to $\theta_{initial}$ and does not save because there is a slight shift in angular position data when moving the opposite direction. In the future, this shift could be calculated and implemented in the DAP to reduce scan time by ~5%. To scan an area of 140 cm^2 at 2 mm resolution, it takes 1.25 hr (6577 points/hr or ~1.8Hz) and 0.25 hr (33,000 points/hr or ~9Hz) for slow and fast modes, respectively.

3.5. Weatherized Computer

For laboratory experiments where space and time are relatively unlimited, the size and amount of equipment is often irrelevant. However, space and time are often limited for field studies; the size and amount of equipment is inversely related to how efficient a field study goes. The ideal means of collecting data is with a laptop; however, standard affordable laptops have no serial communication ports to efficiently communicate with the LR and PTU. Both USB-to-Serial and PCMCIA-to-serial adapters were attempted but would not respond effectively in MS-DOS; when running the DAP in Windows XP through an MS-DOS terminal, only about 1/5th of the data was coherent. Therefore, a

small fan-less industrial computer was built into a briefcase-sized box (Fig. 3.3) to eliminate the need for bulky equipment and extra time being spent connecting cables. Since proposed future studies include coupling the raindrop size distribution of a rainstorm from a disdrometer with the surface roughness changes from the TLS or documenting the evolution of a developing rill, a waterproof/dustproof, hardened computer was needed that could withstand repeated outside use.

Figure 3.3 Bulky monitor/CPU (left), weatherized computer (left-center), weatherized computer with monitor for camera (right-center), and side view of closed box (right)

3.6. Cost Assessment

One of the main design requirements for this instrument was to minimize cost. Since there were many iterations of the TLS and the specific applications it was used for determine what components were needed, two itemized cost assessments were tabulated and are presented in table 3.3. For example, when using the TLS in a laboratory setting, the ~$1252 weatherized computer discussed in section 3.5 was helpful but not needed. The camera shown in figure 3.2 (and associated power supply, cabling, and extra monitor) are not taken into account in the cost assessment since it is no longer

manufactured and is only used to aid in following the laser dot when setting up each survey. The standard PTU was chosen for its ruggedness and ability to have multiple sensors mounted (i.e. laser and camera); however, it could be replaced by a miniaturized version (without camera mount) to reduce the cost by $2000. Depending on the application (or desired vantage point), the scientific tripod could be replaced by a standard surveying tripod to reduce the cost by ~$260. The connection plates briefly discussed in section 3.3 and time for a machinist to make them were assumed to cost a total of $100. The watertight aluminum box (Fig. 3.2) used to house the power supplies and associated cabling could be replaced with a lighter-weight watertight plastic box to reduce the cost by ~$220. The time-cost of building the computer and power boxes as well as the cost of all electrical connectors is not included since they are highly variable and also depend on the skill of the manufacturer.

Table 3.3 Itemized cost assessment for standard (left) and reduced price (right) components

	Cost		Cost
Hardware		**Hardware**	
Laser (Acuity AR1000)	$ 2,000	Laser	$ 2,000
Pan-tilt Motor (FLIR PTU-D48)	$ 4,500	Pan-tilt Motor (Mini)	$ 2,500
Scientific Tripod (Campbell CM6)	$ 456	Surveying Tripod	$ 200
Tribrach & Adapter (Seco)	$ 135	Tribrach & Adapter	$ 135
Connection Plates	$ 100	Connection Plates	$ 100
Watertight Aluminum Box	$ 271	Watertight Plastic Box	$ 50
Computer Box		**Computer**	
8" LCD Monitor (LCD8LVGA)	$ 205	Standard Computer	$ 200
1.5amp Monitor Power Supply	$ 22	Standard Monitor	$ 100
Waterproof Case (NANUK 915)	$ 90	Total Cost =	$ 5,285
Wireless Keyboard (WetKeys EKW-108)	$ 59		
Mini Industrial Computer (Advantech ARK-3202)	$ 876		
Total Cost =	$ 8,714		

CHAPTER 4. CALIBRATION AND VALIDATION

4.1. Offset Correction

Since distance is not measured from the origin of the PTU axes, (the origin is offset (dX=136 mm, dY=60 mm, dZ=8.25 mm as shown in Fig. 4.1) an adjustment must be applied to obtain precise measurements. To check the accuracy of the calibration, coordinates of 4 points with known offsets (h_M) were acquired. The calibrated distance between points (h_C) was acquired by substituting equations 4.1-4.8, which apply the offsets and convert from spherical to Cartesian coordinates, into equation 4.9. Next, the differences (Δh) between the calibrated distances and measured distances were summed (see equation 4.10) and an Excel goal seek was used to minimize the difference by changing the elevation leveling offset (θ_L). For example, the total summed error in all four positions was 6.7 mm without accounting for θ_L and 1.7 mm with accounting for θ_L. Since the instrument can only be leveled to as good as putting the bubble in the center of the tribrach, there will still be some minor leveling errors. Thus, it is important to check the calibration using the 4-point method placed in the center of the AOI each time a scan is taken. For far scans (>8m), the elevation leveling offset becomes negligible.
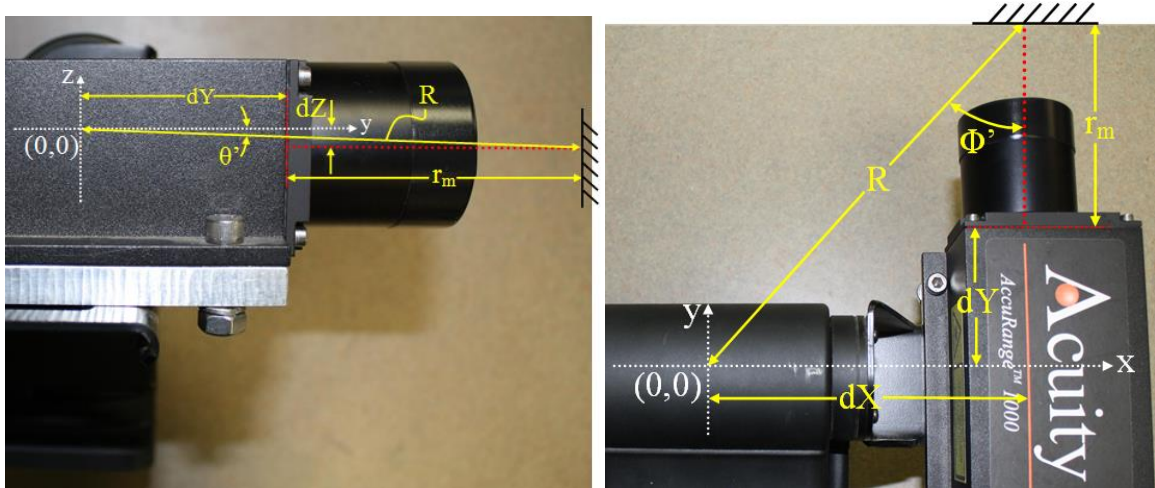
Figure 4.1 Side view shows offsets in x-z direction (left) and Top-down view shows offsets in x-y direction (right)

$$\phi' = \tan^{-1}\left(\frac{dX}{(r_m + dY)\cos(\theta)}\right) \tag{4.1}$$

$$\theta' = \tan^{-1}\left(\frac{dZ}{r_m + dY}\right) \tag{4.2}$$

$$R = \sqrt{(r_m + dY)^2 + dX^2 + dZ^2} \tag{4.3}$$

$$\theta_C = \theta' + \theta_L + \theta \tag{4.4}$$

$$\phi_C = \phi' + \phi \tag{4.5}$$

$$x_C = R\cos(\theta_C)\sin(\phi_C) \tag{4.6}$$

$$y_C = R\cos(\theta_C)\cos(\phi_C) \tag{4.7}$$

$$z_C = R\sin(\theta_C) \tag{4.8}$$

$$h_C(1 \rightarrow 2) = \sqrt{(x_{C2} - x_{C1})^2 + (y_{C2} - y_{C1})^2 + (z_{C2} - z_{C1})^2} \tag{4.9}$$

$$\Delta h = \sum_{i=1}^{4} |h_C(i) - h_M(i)| \tag{4.10}$$

4.2. Acceleration/Deceleration Correction

Since the PTU auto-calibrates upon power-up and the laser rangefinder was calibrated before arrival, the survey mode is sufficient to accurately acquire point locations to eventually yield a digital elevation model (DEM). The elevations in fast and

slow modes are slightly shifted from those in survey mode and need to be corrected in order to obtain an accurate DEM. This is due to small timing errors between the time the angular positions are measured in a moving system and the time when the distance measurement is made. The offsets ($\theta*$) were computed using principles of optimization; a 2-dimensional area was profiled by fast, slow, and survey modes, $\theta*$ values were determined by minimizing the sum of the differences (Fig. 4.2). The first and last few points of each slice in a fast scan are inaccurate (Fig. 4.2) and thus are removed. The errors arise because as the PTU accelerates or decelerates, there is a finite time lag between the position when requested and position when determined.
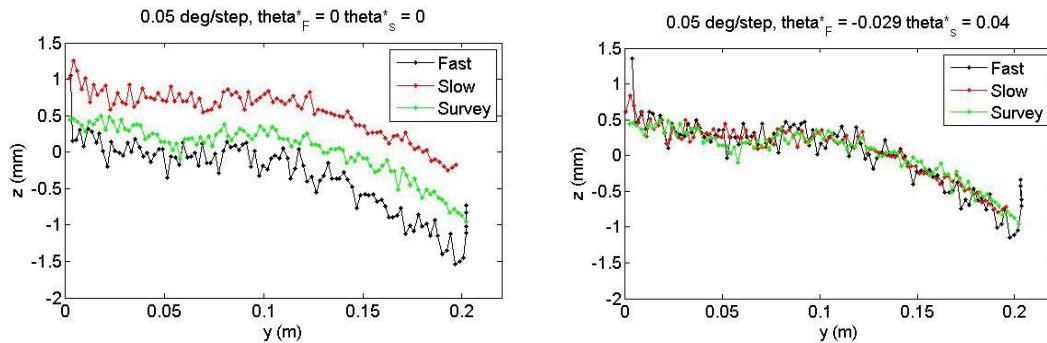
Figure 4.2 Raw data (left) and corrected data (right); the maximum absolute difference in z for fast mode is 0.79 mm and 0.36 mm for raw and corrected, respectively.

4.3. Volumetric Uncertainty Test

Accurately measuring the volume of material eroded from various environmental processes is important because the rate of erosion is often scaled up from model to actual conditions or scaled up with time; therefore, associated errors are scaled accordingly. The objective of this exercise was to determine how certain the TLS can profile and

subsequently compute the volume of blocks with varying size and texture (Fig 4.3). Each block had a flat bottom to keep the estimate simple. The actual volume of angular blocks was computed using a caliper. The volume of smooth wooden blocks was computed by submerging each block in a graduated cylinder and measuring the displacement; nonzero uncertainty from this method was expected since the beaker wasn't perfectly circular. This method is also not highly accurate since it was difficult to submerge the wooden block while simultaneously measuring the displacement. To reduce errors due to floating, a bucket with a small wooden structure (to give the block depth) was smoothed with molding clay and filled with a Plaster Paris mixture. Once dry, the molds were taken out and painted to minimize the amount of open pores that could absorb water. Next, the blocks were submerged in water and the water level was recorded once bubbles ceased coming off the surface (by using TLS to get the distance and elevation to a small piece of paper that was floating on the water). Finally, the blocks were removed from water and an accurate graduated cylinder was used to add known amounts of water until the submerged block water level was reached.

Figure 4.3 Blocks of various sizes and textures used to assess uncertainty; angular (left), smooth wood (center), and plaster (right)

Next, each object and its bare footprint were scanned from two different positions to obtain a full 3D point cloud representing the object. Point clouds were then referenced and cropped using MATLAB. Mixed-edge effects were removed using Cloud Compare by highlighting and deleting points such as those in the yellow circles of figure 4.4. Next, the point cloud was converted to a triangulated irregular network (TIN) and subsequently a raster (aka a DEM) with 1mm resolution, using ArcGIS. The floor raster was subtracted from the object raster to yield the object in absolute coordinates. Then the elevation of each raster element was multiplied by its constant area (1 mm^2) and summated to yield the volume of the object. This process was also performed with a block submerged under water (see section 4.2).

Range inaccuracies can be seen near the edges of angular objects as described in section 3.1. The mixed edge effects are shown in figure 4.4 from a survey of a rectangular aluminum brick (center block of Fig. 4.3 left); the data points in the yellow circles don't represent a real surface but arise because the laser range finder averages between the edge of the brick and the floor underneath it.
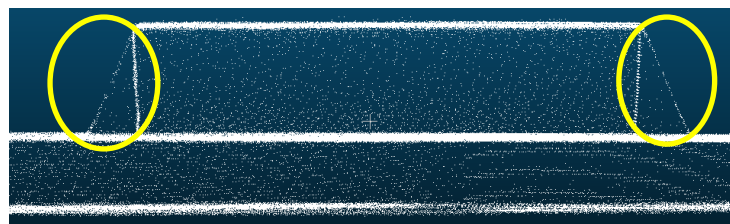
Figure 4.4 Front view of a survey of a rectangular aluminum brick to portray the extent of mixed-edge effects

Various angular and smooth objects were scanned to eventually compare the volume measured to the actual volume; the results are shown in figure 4.5, where the

error computed assumes that the measured volume is the actual volume (opposed to the laser-scanned volume). Angular blocks have the highest error due to mixed-edge effects, but the error decreases with increasing volume. Smooth wooden blocks have less error than angular blocks and also roughly follow the trend of decreasing error with increasing volume. The plaster blocks have significantly less error with the highest being 0.45% and decreases towards to zero for larger volumes. To achieve smaller errors, this exercise should be performed again with more emphasis on rigorously removing all mixed-edge points and using a more precise method of measuring the actual volume.
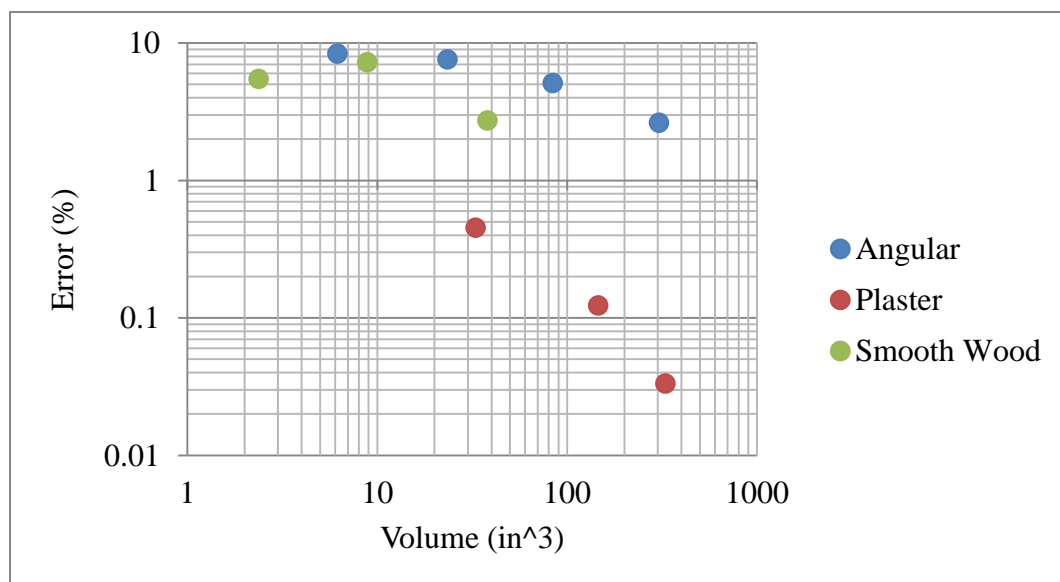
Figure 4.5 Graph of actual volume vs. error for various types of blocks

4.4. Underwater Testing

One of the major benefits of the SExI over other commercial TLSs' is that the LR can measure distance through water. In order to accomplish this, the water must be clear enough to see through to the bottom (i.e. low turbidity) and have no direct sunlight on it.

The raw data can be corrected using Snell's law (eqn. 4.11) which describes the bending of a wave when it crosses the interface between two different media (air and water in this case). The index of refraction for air and water is 1 and 1.33, respectively. In order to apply the correction, the distance and elevation angle to the water surface must be known to compute the vertical distance from the TLS origin to the water surface (Z_w). The correction equations were modified from those published by Smith et al., 2012.

$$\frac{sin\ \theta_a}{sin\ \theta_w} = \frac{1.33}{1} \tag{4.11}$$
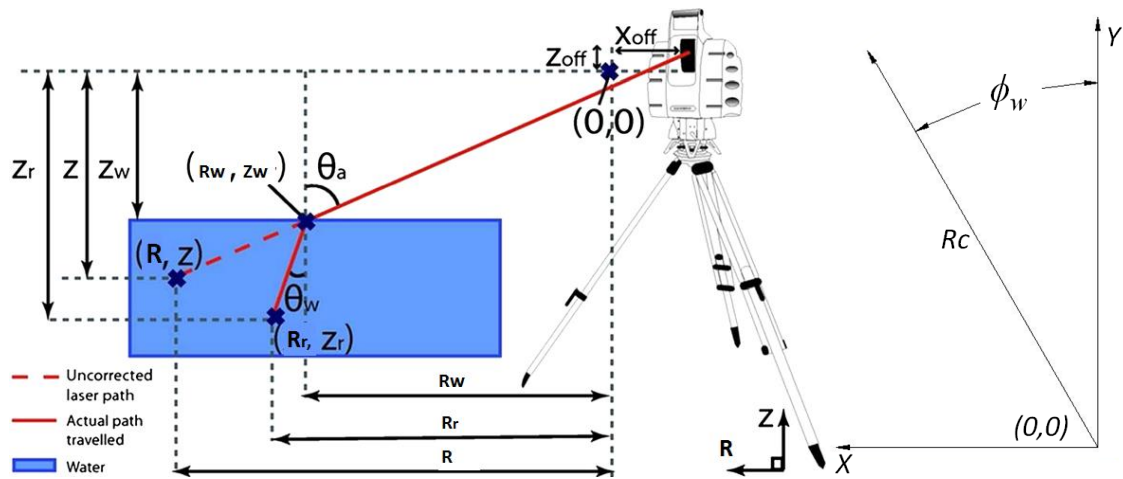
Figure 4.6 Schematic of the geometry of the underwater refraction correction variables (left, modified from Smith et al., 2012) and schematic of the plan-view geometry (right)

Equation 4.12 is used to calculate the angle ϕ_w perpendicular to the TLS origin to the line-of-sight (Fig. 4.7) using the calibrated values from section 4.1.

$$\phi_w = \tan^{-1}\frac{x_c}{y_c} \tag{4.12}$$

The resultant vector (R_C) is obtained using the Pythagorean Theorem as shown in equation 4.13.

$$R_C = \sqrt{x_c{}^2 + y_c{}^2} \tag{4.13}$$

From figure 4.7, the angle of incidence θ_a is given by equation 4.14.

$$\theta_a = \tan^{-1}\frac{R_C}{z_c} \tag{4.14}$$

Equation 4.15 is obtained by rearranging equation 4.11.

$$\theta_w = \sin^{-1}\left(\frac{\sin\theta_a}{1.33}\right) \tag{4.15}$$

The distance from the laser to the water surface (R_w) is obtained using equation 4.16.

$$R_w = z_w * \tan\theta_a \tag{4.16}$$

The vertical distance from the TLS origin to the underwater coordinate is given

using equation 4.17.

$$z_r = \frac{\cos\theta_w(R_c - R_w)}{1.33\sin\theta_a} + z_w \tag{4.17}$$

The horizontal distance from the TLS origin to the underwater coordinate is given

using equation 4.18.

$$R_r = \frac{(R_c - R_w)}{1.33^2} + R_w \tag{4.18}$$

The refraction-corrected y-coordinate is obtained using equation 4.19 by

accounting for the angle of the resultant.

$$y_r = R_r\cos\phi_w \tag{4.19}$$

The refraction-corrected x-coordinate is obtained using equation 4.20 by

accounting for the angle of the resultant.

$$x_r = R_r\sin\phi_w \tag{4.20}$$

It is important to note that slight modifications on the order of a few millimeters

might need to be applied depending on water depth and TLS setup. Therefore, it is vital

to check the uncertainty of each underwater experiment by comparing positional

information of a scan taken dry and underwater.

4.4.1. Block Testing

To test the underwater capabilities, a rounded wooden block was fastened to a board and weighted down to prevent floating (Fig. 4.7). First, the block was scanned without any water in the bucket. After about 10" of water was added to the bucket, a piece of paper was floated on the top and the laser was used to precisely measure the vertical distance from the laser to the water that was necessary to apply the underwater correction. As shown in figure 4.8, there was only ~5% volumetric difference between the dry and bathymetric surveys. Most of the difference is suspected to be caused from the block shifting slightly when water was added to the bucket. This may be due to the fact that the bucket deformed as water was added (Fig. 4.7). In the future, this test should be redone with the block fastened to a rigid bucket to eliminate shifting errors.

Figure 4.7 Dry (left) and wet (right)
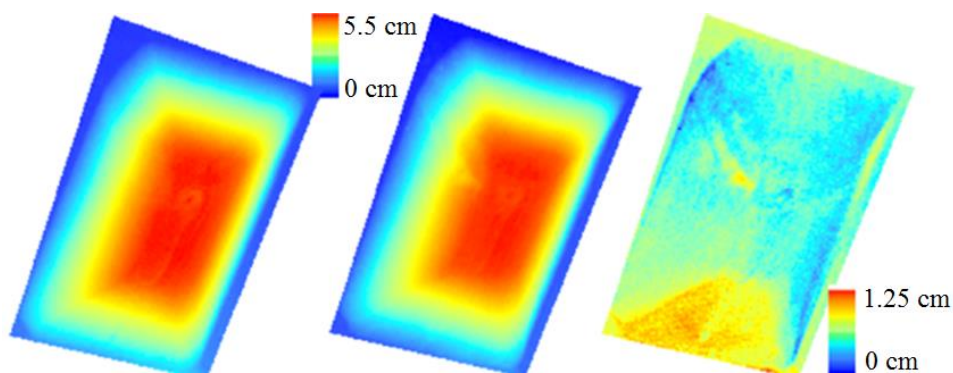
Figure 4.8 Dry (left), wet (center), and difference (right)

4.4.2. Ralston Creek Stream Profiling

This survey was taken on March 24, 2012 around 6:50pm at Ralston Creek due south of the intersection of E. Prentiss and S. Linn Streets. The skies were blue and the sun was shining, but not in the direct vicinity of the river AOI (Fig. 4.9). Since the water surface consisted of moving ripples, 5 scans were repeatedly taken over the same area at 0.05°/step (Fig. 4.10) to average out these fluctuations. In order to correct for the water surface, coordinates of two points (one on each side of the creek) just above the water surface were recorded and averaged. Note that the coordinates in Figure 4.10 are referenced to the scanner origin.

Figure 4.9 Ralston Creek line-of-sight laser survey
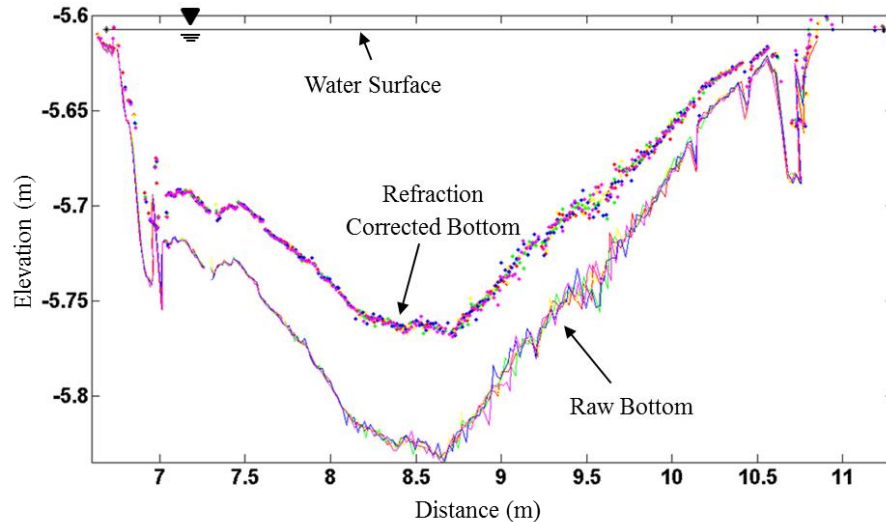
Figure 4.10 Survey of Ralston Creek with the dots representing the corrected bottom surface and lines representing the raw (uncorrected) bottom surface

4.4.3. Underwater Culvert Scanning

Culverts are a type of conveyance structure allowing water to flow around or underneath various obstructions (such as bridges, roads, train tracks, etc.). Culverts are highly susceptible to scour and sediment deposition because they have sudden expansions and contractions. Expansions slow the flow velocity and create areas of circulation (Fig. 4.11) when followed by a contraction. The spatio-temporal distribution of sediment is desirable in understanding the scour process. Examination of these processes requires high resolution measurements. The TLS was deployed to profile the three-box-culvert at various times of constant flow on July 27, 2011.

Figure 4.11 Three-box-culvert in Model Annex Flume
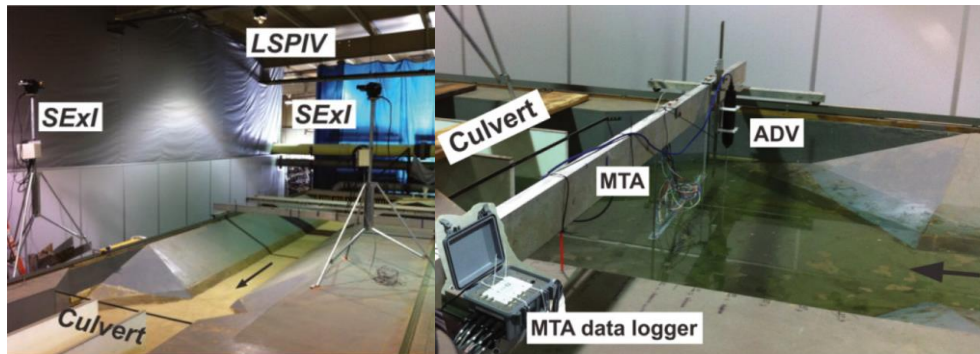
Figure 4.12 Experimental setup: 2 TLSs and LSPIV mounted to ceiling (left) and SeaTek ultrasonic distance sensor and Vectrino 3-component velocity gauge mounted on a movable carriage (right) (Ho et al., 2013)

The area upstream of the three-box-culvert was designated as the AOI with an allowable 20 minutes per scan. The tripod and components were set up directly downstream of the culvert expansion as shown in figure 1. After the laser was leveled, azimuth and elevation ranges were defined to be 66→-32 and -55→ -70 degrees, respectively (layout of data shown in table 4.1). An increment of 0.65 degrees per step was used to accomplish the time requirement; each scan took ~13 minutes to obtain ~4000 points including ~700 outliers (primarily due to poor visibility in the water). The water level was obtained by floating a piece of paper on the surface and recording the

distance and elevation. Finally, ArcGIS was used to create a raster (pixel-image) of each

scan for visualization of the scour-deposition process.

Table 4.1 Layout of data (note that water level must be manually entered into table)

Point #	Azimuth (°)	Elevation (°)	Range (m)
1	66	-55.096	3.55
2	66	-55.276	3.16
3	66	-55.894	15.000
.	.	.	.
.	.	.	.
.	.	.	.
3927	-31.1170	-69.9860	3.5690
Water Level	49.992	-57.064	3.513

The experimental results show a trend from a ~flat initial bed to large oval-shaped

deposition areas which can be seen by comparing figures 4.13. Other instrumentation

data was not accessible to provide proper validation or to evaluate uncertainty. The

experimental results contained a high amount of noise values, many of which can be

attributed to placement of the SeaTek and Vectrino directly upstream of the culvert,

which created turbulence. This induced air entrainment and sediment to become

suspended, which is why the images in Fig. 4.13 are small in comparison to the actual

culvert area (the laser could not penetrate the water further than ~1 horizontal meter

away). Another source of error is the fluctuating water surface throughout each scan or

between them. Since the fluctuations were small in comparison to the overall differences

in sediment distribution, they were neglected.
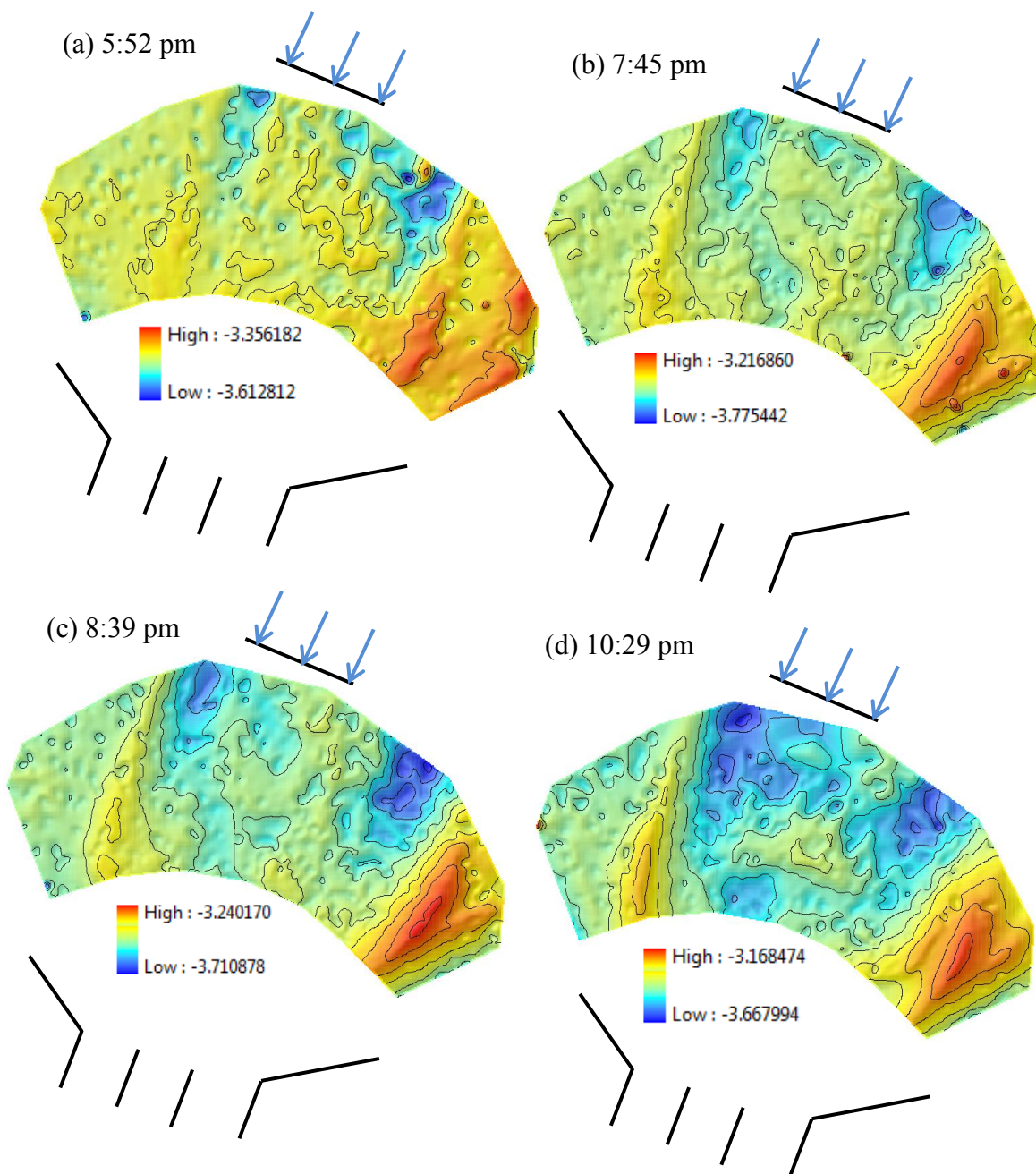
Figure 4.13 Initial bathymetry with a 25.6 cm variation in elevation taken at 5:52pm (a), 55.8 cm variation taken at 7:45pm (b), 47 cm variation taken at 8:39pm (c), 49.9 cm variation taken at 10:29pm (d). For reference, the black lines indicate the approximate location of the piers.

CHAPTER 5. EXPERIMENTS AND APPLICATIONS

The TLS was used on a variety of indoor and outdoor experiments to document changing conditions in stream banks or erodible beds. From these experiments, the TLS has proven its capabilities to be used in many different conditions to acquire high resolution data of the area of interest. Some of the applications it was used for are summarized below.

5.1. Priest Rapids Tailrace Model Scour Summary

In this experiment we measured the scour potential of an erodible bed that was associated with the probable maximum flood (PMF) conditions. To do so, two TLSs were set up to profile the erodible bed prior to and after the flow being set and run until bed stability became apparent. The TLS data was referenced to the Columbia Dam geographic system and combined to yield high resolution topographic maps of the bed conditions; the combined and scaled resolution was set at 1ft pixels (5mm model) which is smaller than the minimum point-to-point distance of one scanner because point density increases considerably with the addition of a 2nd TLS. Specific details of this experiment can be found in appendix A (Plenner et al., 2013 pending).

5.2. Streambank Retreat Monitoring at Clear Creek Summary

In this experiment we profiled a ~9 m wide portion of a meandering bend of Clear Creek on two separate occasions. Bank profiles were acquired on July 2012 and July 2013; the resulting subtraction of the data yielded a mean stream bank retreat rate of

2.131 m/yr with a maximum of 3.7 m at the upper portion of the bank. The amount of volume change (61.4 m^3) over the course of a year is significant from both stream morphology and water quality perspectives; it is equal to dumping ~8-standard 10 yd^3 dump trucks of sediment into the stream. Specific details of this experiment can be found in appendix B (Plenner et al., 2013 pending).

5.3. Scour Assessment of Self-Cleaning Culvert

To determine the effectiveness of sediment passing through and not depositing in box culverts, the TLS was used to map the bed of a 1:5 scale culvert model. Two TLS stations were used to see behind the box walls and yield higher resolution data. Also, a new algorithm to reduce scan time and increase efficiency was born. More information about this experiment can be found in appendix C (Muste, 2009; Ho et al., 2013).

5.4. Streambank Retreat Monitoring Behind UNFI

In this experiment, we profiled a small stream that meanders through a riparian corridor adjacent to an industrial area with many impermeable surfaces. The area of interest was small and only one TLS station was used to profile the bank since there were no surface features blocking the line of sight. Scans were taken from June through March; however, little bank changes were noticed. More details of this experiment can be found in appendix D.

CHAPTER 6. CONCLUSIONS AND OUTLOOK

Due to the need for an inexpensive, robust, and customizable terrestrial laser scanner to aid in the investigation of fluvial and hydraulic phenomena, the Surface Examining Instrument was developed. After initial development and calibration, the SExI has been used to investigate objects with high resolution underwater, scour conditions with the addition of a fish ladder and in a self-cleaning culvert, and streambank erosion for two field sites. The instrument can resolve surface features as small as a few millimeters with high accuracy. For instance, the volume of a small block was measured with an error of 0.035%. These investigations have led to the development of a faster scanning mode, and physical upgrades including addition of a tribrach, camera, and weatherized computer box. The total system cost (of one scanner) is less than $10,000, which is roughly $1/10^{th}$ the cost of an industrial TLS.

In the future, time reduction strategies could be implemented, including calculating offsets to the fast scanning mode to allow data collection in both scanning directions and the algorithm to scan between 4 Cartesian points to avoid redundant data collection. Also, the streambank retreat study at Clear Creek could continue to be performed on an annual basis around late July, when flow levels have receded enough to allow the operator to easily carry the equipment across the river. To continue this study, excavation of the triangulation stakes will most likely be necessary but not exceedingly difficult. The TLS could also be used to aid in more in-depth analysis of bank processes such as slumping, corrasion, or freeze-thaw cycles with the addition of temperature and humidity probes. Lastly, a Standard Operating Procedure (SOP) manual will be written and available to anyone interested in using the TLS.

APPENDIX A.

Priest Rapids Tailrace Model Scour Test

Abstract:

Large-scale laboratory models of hydraulic structures are used to assess and test new system designs prior to implementation. Some of these models are built with an erodible bed to examine the scour potential related to operations and design floods. Typical methods of documenting bed conditions (such as: photogrammetry, point gage, and total station) are best suited for small-scale models. While terrestrial laser scanners (TLSs) are fast and accurate, they are often too expensive for limited use projects such as large-scale laboratory models. Therefore, a new affordable and robust terrestrial laser scanner was developed and utilized for a large-scale laboratory model of the Priest Rapids Dam located on the Columbia River, Washington. In order to aid in the design of means to enhance the passage of juvenile salmonids (smolts) migrating downstream, a comprehensive 3-D physical model of the tailrace of Priest Rapids Dam was developed. Among the many design challenges associated with this project, one area of interest was to investigate the scour potential within the tailrace, associated with the probable maximum flood (PMF) conditions, utilizing the model's erodible bed.

Introduction:

Laboratory models (specifically of dams, spillways, fish bypass structures, etc.) are often used to assess the hydraulics of a new design prior to implementation. Some laboratory models are built with an erodible bed to study the amount of erosion or deposition due to design flows. Gross et al. (2010) used a small-scale physical model (0.61 m x 0.91 m) to simulate levee erosion and used an expensive commercial laser scanner to document the rill evolution. Tian et al. (2010) used a medium-scale flume (2.44 m x 1.22 m) to measure scour depth around hydraulic structures using a laser light sheet and digital camera. Medium-scale flumes (<4.18 m x <4.18 m) have also been used (Rieke-Zapp et al., 2001; Rieke-Zapp et al., 2005) to measure soil surface roughness and erosion by employing digital photogrammetry. Point gauges (Hong 2005; Hong et al., 2010) have often been used to measure local scour conditions but are slow and limited to small areas. The acquisition of high resolution measurements to yield a digital elevation model (DEM) is important in quantifying the extent of erosional/depositional processes and validating the laboratory model design. For small to medium-scale flume-based experiments, digital photogrammetry, a track-mounted laser point gage, or a laser light sheet are most often used. For larger-scale models, a total station or terrestrial laser scanner (TLS) is more often utilized. However, the use of a total station to survey a large areal extent at high resolution is time-consuming and arduous since traverses must constantly be repositioned so the reflector-holder does not disturb the erodible bed. Commercial TLSs are fast and can acquire the full extent of the model at high resolution, but are often too expensive to be used solely for limited-use laboratory models. The purpose of this study is to present a simple, low-cost, and robust TLS that is most optimally used for large-scale laboratory models with an erodible bed feature.

Experimental Setup and Procedures

In order to aid in the design of means to enhance the passage of juvenile salmonids (smolts) migrating downstream, a comprehensive 3-D physical model of the tailrace of Priest Rapids Dam was developed. The Priest Rapids Tailrace Model (Fig. A.1) was built to model the Priest Rapids Dam located on the Columbia River in Grant County, Washington. One use of the model was to assess the scour potential due to the probable maximum flood (PMF) of 37,661 m^3/s with a newly designed 3-bay fish bypass in operation. Since the erodible bed portion of the laboratory model is large (8.23 m x 3.66 m), both digital photogrammetry and a track-mounted laser scanner aren't feasible. The typical means of acquiring bed elevation information for a model of this size is using a total station.

Figure A.1 Photographs of initial bathymetry modeled from a multi-beam hydrographic survey (left) and final bathymetry after the PMF (right)

We employed the newly built TLS to assess the scour potential downstream from the Priest Rapids Dam Spillway Model with the fish bypass in operation. The initial bathymetry was modeled at 1:64 scale from a combination of available field and model data; 179 grade stake locations were utilized to create the erodible bed of a gravel-bentonite mixture (Fig. A.1). The initial and final beds were scanned using two TLSs at

different locations; the combined result transformed and scaled up to the Columbia Dam geographic system (NAD 27) is shown in Fig. A.2. All transformations were applied using a program developed at U.T. Dallas (White & Cline, 2009) by deriving transformation parameters corresponding to a least-squares tiepoint alignment procedure. Each scan was set at 0.3°/step to obtain resolutions in the range of 10-65 mm (depending on distance from the scanner), containing ~400,000 points (~11.5 Mb) and took ~12 hours using the slow mode. Two TLSs were used to both increase spatial resolution and see the full extent of the scour holes that might have been missed due to the shadow zone of a single TLS; the combined and scaled resolution was set at 1ft pixels (5mm model) which is smaller than the minimum point-to-point distance of one scanner because point density increases considerably with the use of a 2nd scanner. Following the initial bed survey, the total flow was set at the PMF and ran for 158.5 model hours until bed stability was apparent. The final bed was scanned using two TLSs' at approximately the same positions as the initial scan positions; the combined result transformed to the Columbia Dam geographic system is shown in Fig. A.2.

Experimental Results and Discussion

The TLS surveys were validated on the final bathymetric survey using a total station; elevations from 230 total stations points were compared to those from the TLS to yield an average difference of -0.18 ± 0.74 m (-0.28 ± 1.16 cm model). While the error is high, the difference was within the grain size distribution of the aggregate used to make up the erodible bed. More accurate analysis routines that account for laser offsets (see calibration procedures) have been developed after the completion of this project; the error would be significantly less if the data were to be reprocessed.
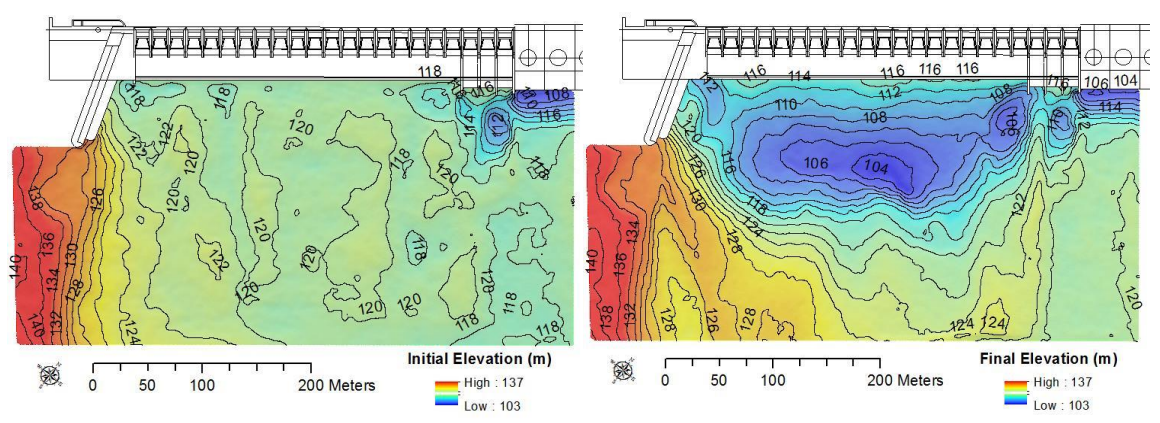
Figure A.2 Initial (left) and final (right) bathymetry from the TLS for PMF scour test
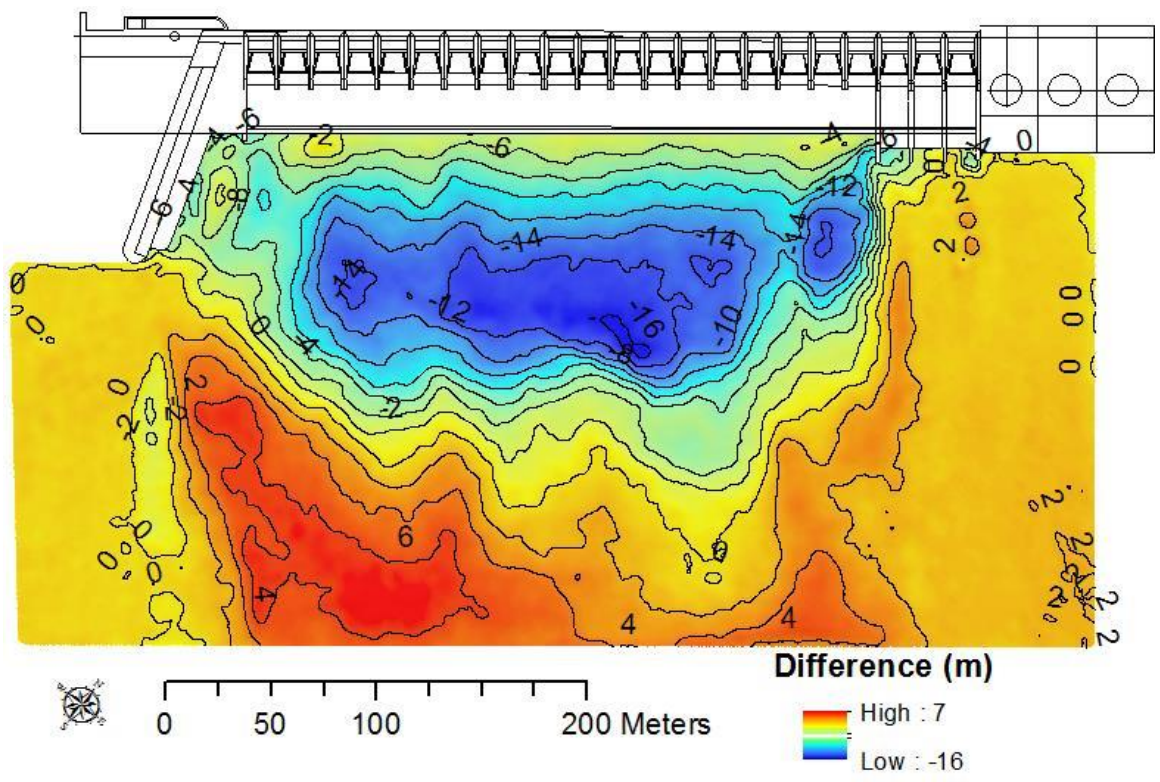
Figure A.3 Difference plot – final minus initial bathymetry; negative and positive values indicate scour and deposition, respectively

Conclusion

Considering the fact that the use of large-scale laboratory models is limited and even less of them employ an erodible bed that are often used only a few times throughout the model life, resources to purchase an expensive terrestrial laser scanner are rarely found. Therefore a simple, affordable, and robust TLS was developed. While the SExI may not be as fast as commercial TLSs, large-scale laboratory models are most often built and tested indoors and therefore are not stringently limited by time. For the Priest Rapids physical model discussed above, the scans were set up to acquire data throughout the night, with no delay to the project schedule. Since unlimited time is not foreseen for future outdoor projects, the fast scanning mode was born. Utilizing a TLS for the measurement of scour for large-scale laboratory models is advantageous over conventional point methods in that it can precisely capture the spatial variability of scoured sediment non-intrusively, highly resolved, and with minimal time and effort.

APPENDIX B.

Streambank Retreat Monitoring at Clear Creek Summary

Abstract

High resolution measurements of streambank retreat (SBR) rates are important for engineering applications such as infrastructure planning and stream restoration. Conventional methods of measuring SBR such as erosion pins or total stations lack sufficient point density to accurately capture the spatial variability of bank retreat over an entire streambank surface. We present a newly developed Terrestrial Laser Scanner (TLS) that is affordable, robust, and simple. We employed the TLS to profile a 9-m wide portion of a meander bend on Clear Creek in Coralville, Iowa. Bank profiles were acquired on July 2012 and July 2013; the resulting subtraction yielded a mean SBR rate of 2.131 m/yr, with a maximum of 3.7 m at the upper portion of the bank.

Introduction

Bank erosion is a natural process occurring along all streams that can significantly affect channel size and shape and sediment input. Much of modern infrastructure is built directly adjacent to rivers and streams, many of which are susceptible to significant bank erosion if not properly stabilized. More than $1 billion is spent on stream restoration annually in the U.S. (Bernhardt, 2005) and $16 billion for sediment damages in North America (Osterkamp et al, 1998). Thus, it is important to be able to accurately predict the location and magnitude of bank erosion. Surveying streambanks to document the location and amount of change through time allows for the assessment of the loci and

magnitude of bank erosion; information critical to better understanding of bank erosion mechanisms and improved hazard assessment.

Conventional methods of stream bank surveying include the use of erosion pins, photo-electronic erosion pins (PEEP), total stations, or aerial lidar. Erosion pins are essentially nails inserted into the bank face in a gridded pattern and measured over time to document erosion; they are cheap and easy to use but have poor spatial resolution and can alter bank stability (Lawler, 1993). PEEPs are inexpensive and can provide continuous monitoring of erosion and deposition but also have poor spatial resolution, can alter bank stability, and need to be positioned away from vegetation (Bertrand, 2010). Total stations are best suited for large-scale, low resolution measurements and are most often used to obtain channel cross-sections or to document river flushing of sediment (Brandt, 2004). Aerial LiDAR has been used more recently as it has high spatial resolution and can profile large areas; however, it is expensive and often misses details of the bank face (Nettles, 2010) (Nettles). The newest method of surveying stream banks utilizes a terrestrial laser scanner (TLS) (Nettles, 2010; Nasermoaddeli, 2008; Resop and Hession, 2010); these have high spatial resolution, are fast, accurate, non-intrusive, easily deployable, and automated. However, TLSs and their processing software have been too expensive for limited-use experiments.

This paper documents the development of an affordable TLS and its use for measuring streambank retreat (SBR). SBR is a quantified rate of stream bank change and lateral channel migration that is affected by weather-related events, the detachment and entrainment of soil particles, and mass failure. Knowledge of the rates of SBR are important to be able to predict when or if banks along a stream segment will become

unstable and in need of restoration, and for both sediment modeling and infrastructure planning. Using a TLS, SBR has been quantified for a small stream to demonstrate the potential when compared to manual total station data (Resop and Hession, 2010).

Study Site

Clear Creek, located in Johnson County, IA, is a small meandering stream that is the source of much academic research (Wilson et al., 2007; Papanicolaou et al., 2009) due to rapid changes in flow with each rain event. The drainage area is 254 km^2 at USGS gage 05454300, approximately 3km downstream from the study area. Clear Creek is a sand-bed stream with cohesive banks about 4.5 m high; average baseflow depth of 0.5 m and bankfull width of ~20 m at the study site. The studied bank is on the outside of a meander bend and is composed of approximately 2 meters of oxidized silt loam and silty clay loam alluvium with the surface soil formed in it that grades downward into stratified loamy and pebbly sand alluvium which extend below low-flow stream level. The stream meanders into in an area that had previously been planted with corn and is now in the process of being converted to oak savanna; therefore, there are no mature trees or extensive root systems to stabilize the banks (Fig. B.1). Prior to this study, the bank face was bare with little vegetation and intermittent undercutting. Topographic measurements of the ~9 m wide area-of-interest (AOI) were taken on July 30, 2012 and July 24, 2013.

Figure B.1 Satellite view (Google Earth) of site taken on 9/12 with field-of-view outlined in yellow (left) and image of the initial streambank (right)
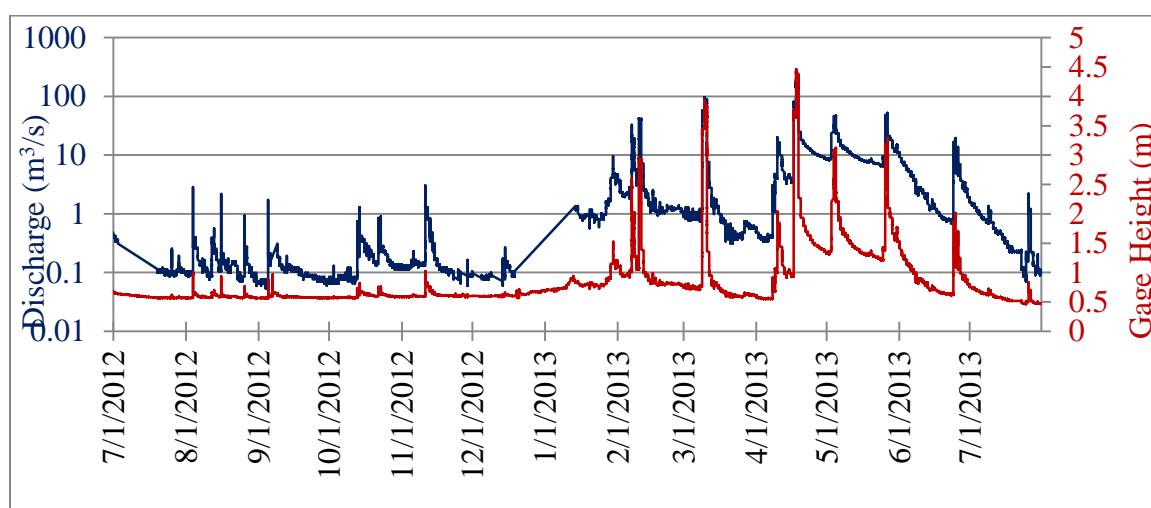
Figure B.2 Discharge (blue) and gage height (red) for USGS 05454300 Clear Creek near Coralville, IA; gage is located ~3 km downstream of the AOI

Field Methods

The TLS was used to scan a 10 m wide portion of the outer bank. Since the AOI is located on the outer bend of the creek, which is also the only feasible access point, field equipment had to be carried across the creek. Therefore, surveys could only be made during low-flow conditions. In order to relate scans over time, 7-1.2 m long wooden stakes were positioned strategically around the site as control points (5 on the

inner bank (point bar) and 2 on the outer bank). Numerous medium and high flow events triggered significant sediment deposition on the inner bank which buried all of the stakes. After triangulation and arduous excavation, the 5 inner bank stakes were located (Fig. B.3 and B.4). Stakes were buried by between 0.3m and 1.5m of sediment, with the deepest ones successively further from the channel.

Since the TLS is line-of-sight, vegetation in the AOI was trimmed down for maximum bank profiling (Fig. B.3). Scan settings were set at 0.05 °/step to yield ~1 cm^2 resolution in the plane of the surface and set to scan a 50° x 17° area from two positions. Multiple scans shifted a fraction of a degree were taken at each position to increase spatial resolution. Scans ran autonomously overnight and lasted ~10.5 hr. each.

Figure B.3 Image of field equipment with 5 of 7 GCPs marked with a yellow star (left) and image of profiled streambank with trimmed vegetation (right)
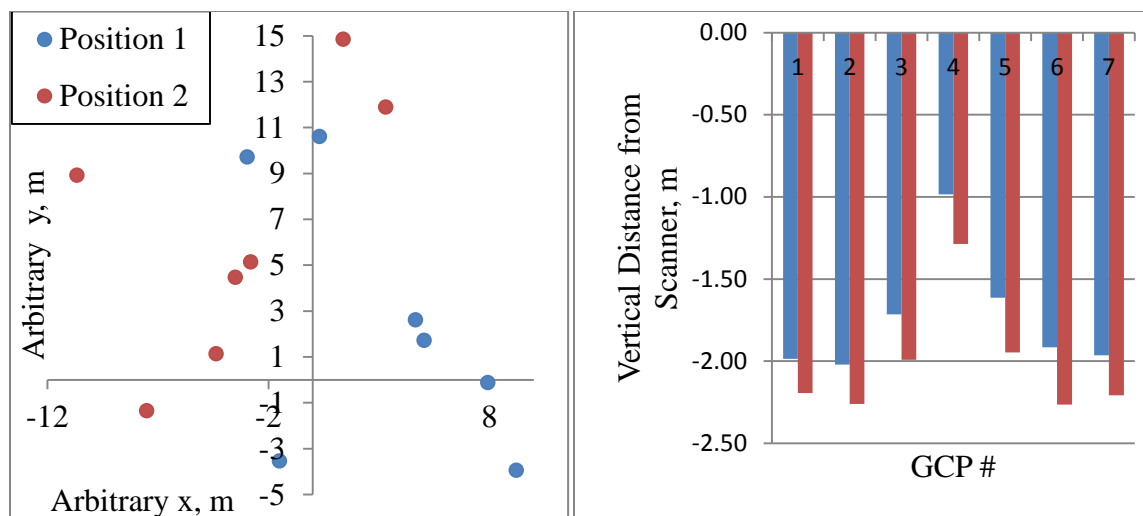
Figure B.4 Plan view layout of GCPs with respect to the origin of scanner in position 1 (left) and elevation distribution of GCPs from respective scanner (right)

Data Analysis

The TLS scan data was processed following the calibration procedures discussed in section 4. Matlab was used to process the raw data and remove easily identifiable outliers based on the use of thresholds. Next, all datasets were referenced to the same coordinate system (of the right position on the 1st scan date) using a transformation program developed at U.T.-Dallas (White & Cline, 2009) by deriving transformation parameters corresponding to a least-squares tiepoint alignment procedure. The root mean square error (RMSE) is a measure of accuracy of alignment between the coordinate systems: it is 0.033 m (1st date left→1st date right), 0.0193 m (2nd date left→1st date right), and 0.0437 m (2nd date right→1st date right).

Each scan position acquired ~1.6 million points over ~29 hours. Since much of the data was clouded with erroneous data points due to vegetation and mixed edge effects shown in Fig. B.5, the typical methods of using thresholds or selecting mass points for

removal wasn't sufficient. Therefore, a new probabilistic approach to classify vegetation was investigated. This new approach, dubbed Canupo (Brodu & Lague, 2012), aimed to characterize features based on various dimensions and scales; line (1D: stems), plane (2D: leaves, water), or whole volume (3D: gravel, bushy vegetation). For this study, Canupo was used to classify vegetation so it could be removed from the scene as seen in figure B.6.
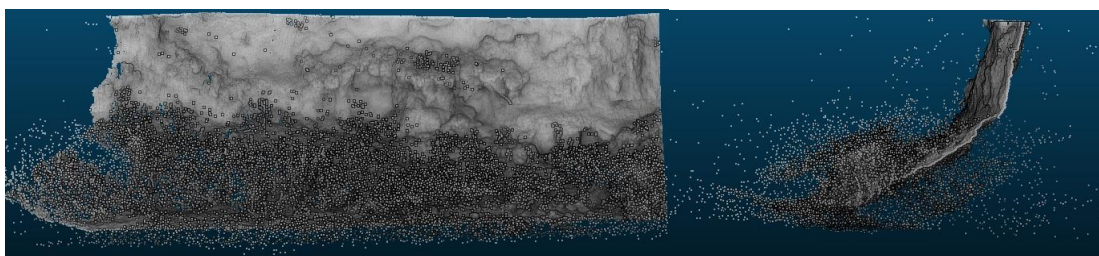

Figure B.5 Point cloud data from the right position; front view (left) and side view (right)
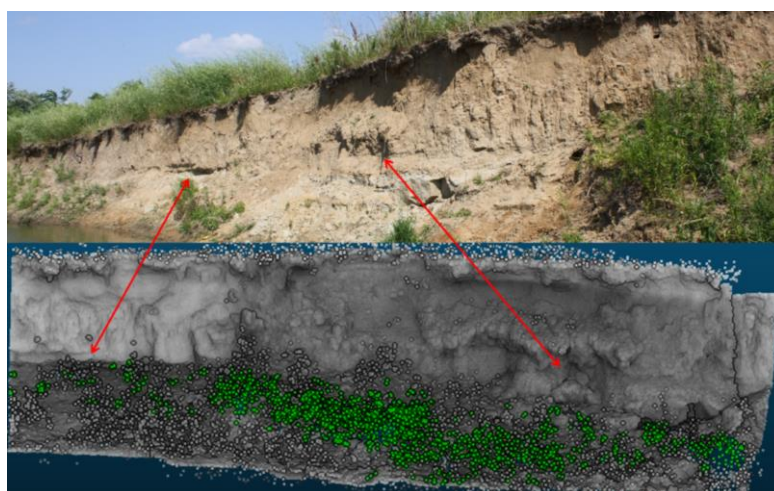

Figure B.6 Picture of AOI (top) and shaded point cloud data (bottom), where green is classified as vegetation using Canupo

Clearly, the scales of vegetation and floor used in Canupo need to be refined in order to more accurately classify all vegetation or non-surface points. Ultimately, the Canupo technique was not used since it failed to remove all the erroneous points from the scene. Thus, mass selection of outliers from various views was used to clean the dataset. CloudCompare, an open-source 3D point cloud processing software, was used to manually remove outliers (mostly due to mixed-edges from vegetation). Finally, ArcMap was used to create DEMs of the data perpendicular to the bank with the elevation being represented as perpendicular distance from the bank (for visualization purposes). Successive DEMs were subtracted to yield a net-change DEM with 1 cm^2 point-to-point resolution of (Fig. B.8). Point values were summed and multiplied by their constant area to yield the net volume change.
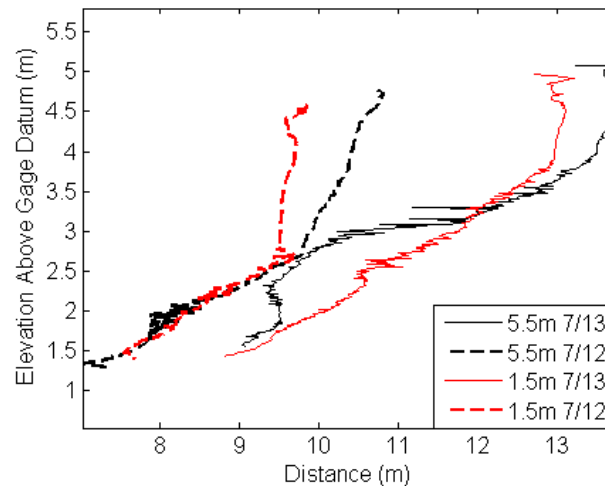

Figure B.7 Selected cross sections at specified distance upstream of the datum; spikes shown on the 7/13 transects are due to traces of vegetation

Results

SBR Rate Comparison

Between the period of July 30, 2012 and July 25, 2013 medium and high flow events contributing to bank undercutting and eventual collapse yielded approximately 61.4 m^3 of eroded sediment. This volume change represents a mean SBR of 2.131 m/yr with the distribution shown in Fig. B.8. The measured SBR rate is within the range of 2-4 m/yr for meander bends of two Iowa rivers (Odgaard); however, the former are significantly larger than Clear Creek (East Nishnabotna River ~50 m top width, 2500 km^2 drainage area; Des Moines River ~200 m top width, 37,500 km^2 drainage area). Clear Creek's high SBR rate at this meander bend compared with rates in the two larger rivers may be a result of Clear Creek's "flashy" discharge. Discharge of Clear Creek can vary by 3 orders of magnitude during peak flows while peak flows of the two larger rivers only vary over about 2 orders of magnitude.
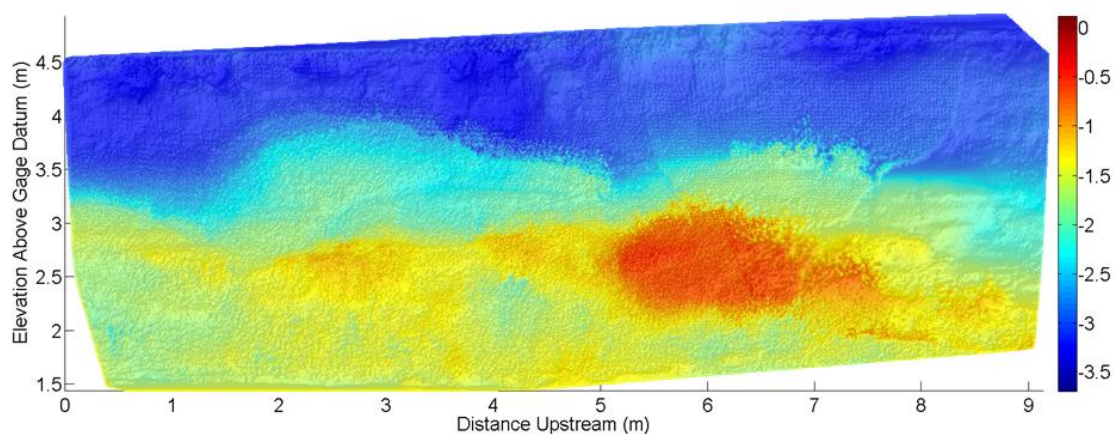

Figure B.8 TLS measured lateral retreat over the bank surface from July 2012 to July 2013 with the color bar indicating SBR (m) from the initial surface

Since the first bank profiles were taken, the stage downstream at the USGS gage has exceeded 2.5 m 5 times with the highest recorded gage height of 4.45 m (Fig. B.2). Each time the stage exceeds ~2.5 m, lateral undercutting followed shortly by mass failure is clearly evident. For the March 10 peak height of 3.94 m, numerous bank sections ~2 m long by ~1 m wide (outside the AOI) were witnessed to collapse, due to cantilever mass failure. These high flows have significantly altered both the AOI and stream segment in general, resulting in making the original low-flow AOI unrecognizable. Example cross sections are shown in Fig. B.7 that compares topographic measurements from two positions upstream of the datum at both scan dates.

Uncertainty Estimate

After applying the speed and offset corrections, the maximum difference between actual and measured results of a profile taken using the TLS is 0.36 mm (Fig. 4.2). We take this as largest potential error per point using fast scan mode; it must then be multiplied by two to account for the subtraction of two profiles taken at different times. Therefore, with a final number of 287,927 pixels with $1cm^2$ area, the differential error is $0.021 \ m^3$. Thus, the total fractional error across the bank area is 0.034%. While this error is small, it is not distributed evenly across the entire streambank; pixels with the largest SBR will have the smallest error.

Discussion

The amount of volume change ($61.4 \ m^3$) is significant from both stream morphology and water quality perspectives; it is equal to dumping ~8-standard 10 yd^3 dump trucks of sediment into the stream. The significant amount of undercutting is

partially due to the lack of bank armoring from roots or energy dissipation from rocks since the substrate is primarily sand. However, some fine-grained material that collapses from the upper part of the bank as flow recedes and doesn't get carried away acts to armor the lower part of the bank until the next high-flow event capable of eroding that material removes it and exposes the easily erodible toe materials.

Since the field equipment had to be carried across the river during low flow, we were unable to acquire bank profiles after each storm event to portray the bank evolution. For future TLS studies of SBR, a stable and non-eroding position for deployment is desirable to be able to document the evolution of the bank through several flow events.

The angular nature of Fig. B.8 is a result of both filtering vegetation out of the scene and of profiling an area (the bank) in a spherical coordinate system that has increasing depth with increasing height above the water. While the SExI is not as fast as commercial TLSs, it is more than capable of scanning large river banks with high spatial resolution at a much-reduced upfront cost. If conventional methods such as erosion pins or PEEPs were utilized for this study, they would have washed away since the amount of lateral migration was larger than the length of the pins used in the point instruments.

Conclusion

In this technical document, we presented a newly designed terrestrial laser scanner that is simple, robust, and affordable for limited-use projects. We then employed the scanner to profile a stream bank prior to and after spring flood flows. Results from the subtraction of profiles and identification of buried stakes show significant and quantifiable lateral migration of the bank and delivery of sediment to the channel. Utilizing a TLS for the measurement of bank retreat is advantageous over conventional

point methods in that it can precisely capture the spatial variability in bank retreat over

the entire streambank surface with minimal time and effort.

APPENDIX C.

Scour Assessment of Self-Cleaning Culvert

After visiting many culverts throughout Iowa, research engineer Marian Muste noted that many culverts are plagued with sediment deposits in the upstream area that partially block flow as shown in Fig. C.1. Muste also noted that "cleanup operations are costly and needed [to be carried out] just two years after a previous cleanup". In order to combat this issue, Muste devised modifications to be made in the upstream area to restore the original (undisturbed) stream prior to culvert construction. To test and optimize the devised modifications, a 1:5 scale three-box culvert model was used (among a 1:20 scale model and numerical simulations not discussed here). Two high resolution non-intrusive instruments, TLS and large scale particle image velocimetry (LSPIV), were applied to concurrently document the coupling between bed morphology and the surface velocity distribution at various times. This experiment was run at constant flow rate using live-bed scour and sediment recirculation for 6 hours to achieve both flow and sediment equilibrium. The initial and final beds were scanned using fast mode and two TLSs at different positions containing ~7000 points each; the result is shown in Fig. C.2. Prior to using the TLS, an ultrasonic depth probe (MTA) using an array of 32 transducers was employed to obtain the bathymetry; this instrument was limited in spatial resolution and was intrusive. The original goal was to use the TLS and LSPIV back-to-back; however, the TLS was unable to acquire data in the deeper parts of the flume due to: high turbidity from the fine sediment used to make up the bed, high Froude number, and residual surface foam from the packaging peanuts used as the tracer particles for LSPIV. Therefore, the initial and final bed surveys were acquired prior to water being added and

after complete drainage, respectively.

Figure C.1 Sediment and vegetation partially blocking a three-box culvert (Muste, 2009)
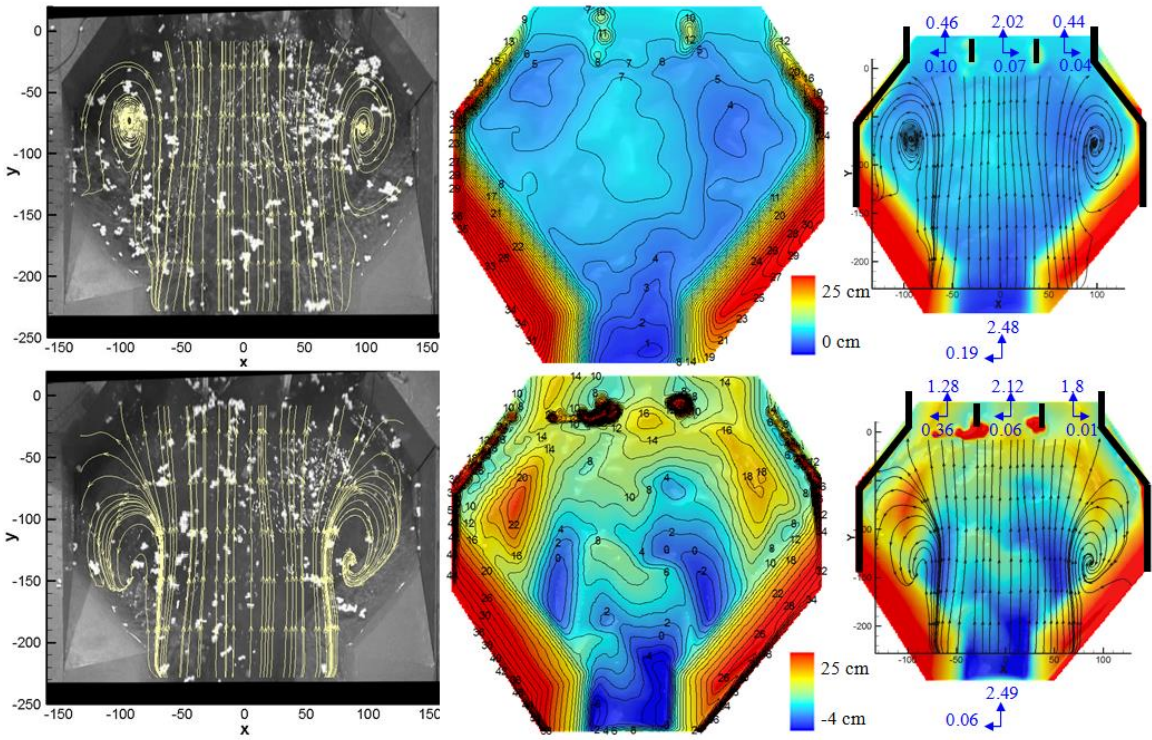

Figure C.2 Streamlines from packaging peanuts as tracer using LSPIV (left), bathymetry from the TLS (center), and streamlines overlaid on bathymetry with mid-depth velocity in fps (right) for initial (top) and final (bottom) conditions

The next part of the project was to survey the three boxes so it could be verified that more sediment was trapped in the outer boxes compared with the center box. Two TLSs were placed on a traverse upstream of the culvert, looking downstream as shown in Fig. C.3. Each scan had ~215,000 points when cropped.
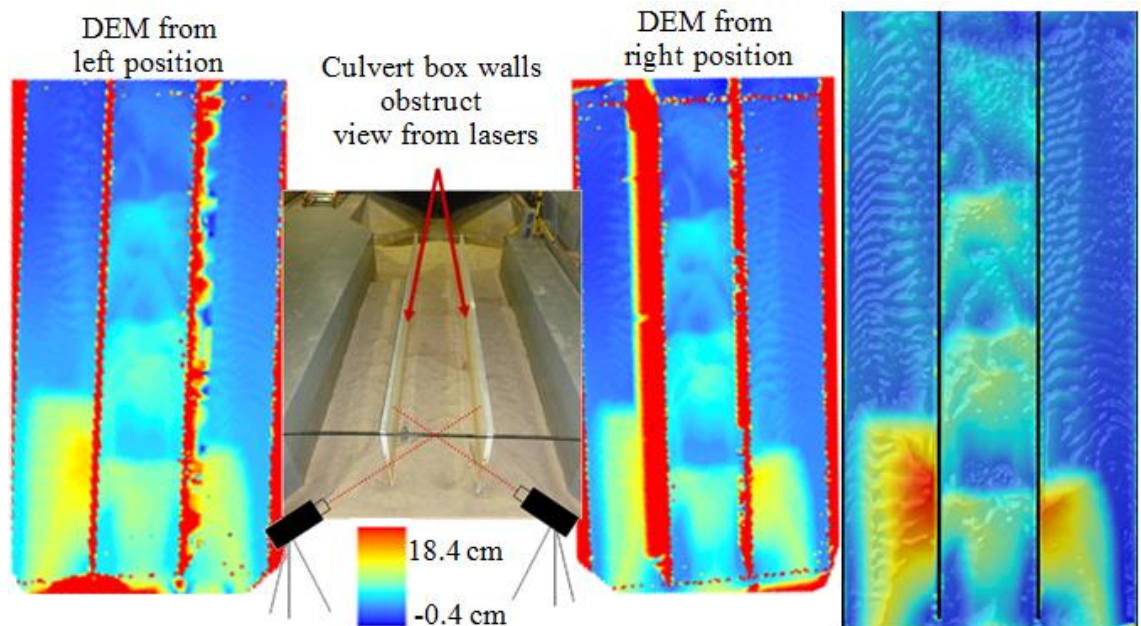

Figure C.3 Two TLSs used to scan the 3 boxes from different positions to see behind the box walls

In addition to learning more about water conditions needed for optimal performance, after completing this experiment it became evident that a new method of data collection to focus on the area of interest is desirable. This would minimize both scan time and quantity of irrelevant data points. This led to the idea of an algorithm to scan between 4 points in Cartesian space, unlike the current DAP that scans between two

elevations and two azimuths in radial space, as shown in figure C.4. The new algorithm

has the potential to reduce scan time by ~34-58%, depending on orientation.
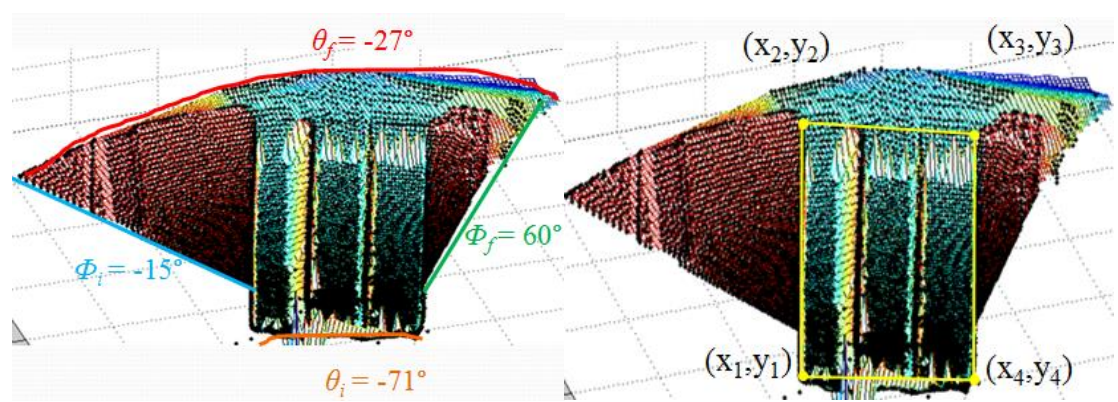

Figure C.4 Current method of scanning bounded by radial coordinates (left) and proposed method of scanning bounded by Cartesian coordinates (right)

APPENDIX D.

Streambank Retreat Monitoring Behind UNFI

Another application using the TLS is the survey of streambanks to quantify the extent of erosion or SBR. Since >\$1 billion is spent on stream restoration annually in the U.S. (Bernhardt, 2005) and >\$16 billion for sediment damages in North America (Osterkamp, Heilman, & Lane, 1998), it is important to be able to accurately predict where and how much erosion occurs.

A small stream with a typical depth < 0.3 m that meanders through a riparian corridor adjacent to an industrialized area has been known to exceed depths of 1.5 m with the slightest amount of rainfall. A specific area where the flow is naturally directed toward a bank clear of woody vegetation was chosen for this study (Fig. D.1). Since the area of interest (AOI) is small (~2.2 m wide by ~1.6 m high) and there were no surface features blocking the line of sight, only one TLS was employed for this study. In order to couple surveys at different times, 4 wooden stakes numbered and labeled with an X were positioned around the site. Before scanning the AOI, the coordinates of the 4 ground control points (GCPs) were recorded.

Figure D.1 Aerial view of site location and schematic of site geometry (left) and picture of experiment setup (right)

Each scan is set for ~3 mm resolution and takes ~4.5 hours to yield ~110,000 points. Point cloud data is converted to an x-z grid (Nasermoaddeli & Pasche, 2008) with 5 mm spacing to allow for DEM subtractions. Subsequent profiles are subtracted and summated to yield the volume eroded (V_E), volume deposited (V_D), and net volume change ($\Delta V = V_D - V_E$). The root-mean-square (RMS) represents the error of transforming the 4 ground control points (GCPs) at subsequent times. The amount of SBR represents the net volume change per bank face area. Surveys from various dates are shown in Fig. D.2-3 using Cloud Compare, an open-source 3D point cloud and mesh processing software.
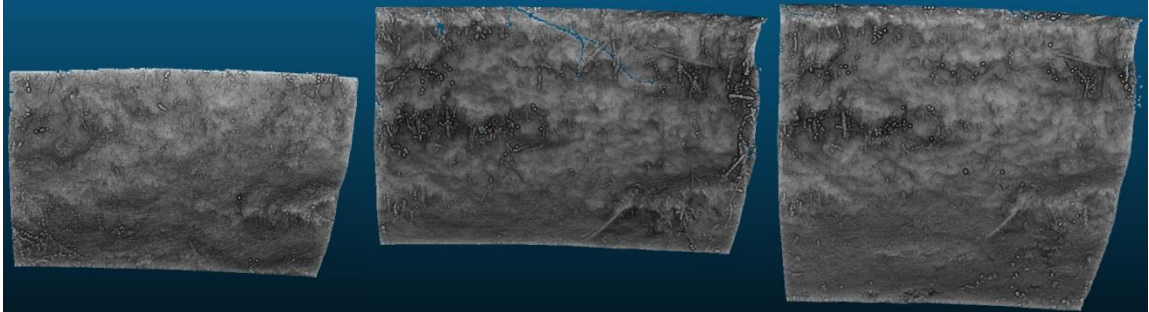
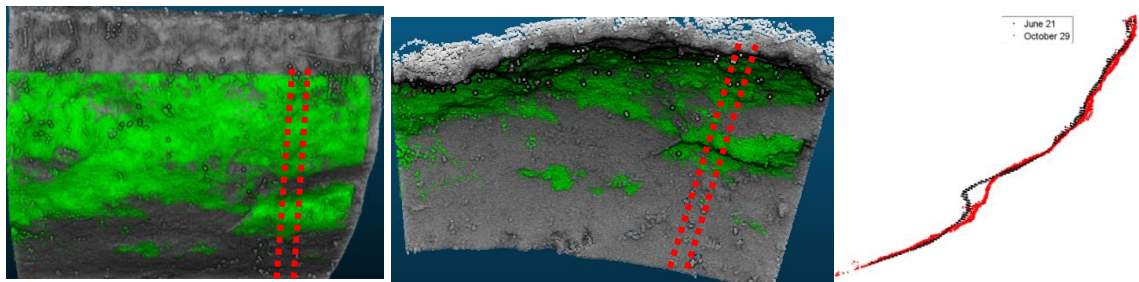Figure D.2 Surveys from the TLS on June 21 (left), August 30 (center), and October 29 (right) of 2012.

Figure D.3 Scan taken in June (green) and October (grey) looking from front (left), top (center), and cross section of scan between the dotted red lines where black dots represent June scan and red dots represent the October scan (right)

The DEMs of difference (DoD) are shown in Fig. D.4 between various dates. Note that the RMS error (Table D.1) is an order of magnitude higher between Feb and Nov surveys, which could be due to debris carried with high flows bumping into or slightly shifting the stakes.
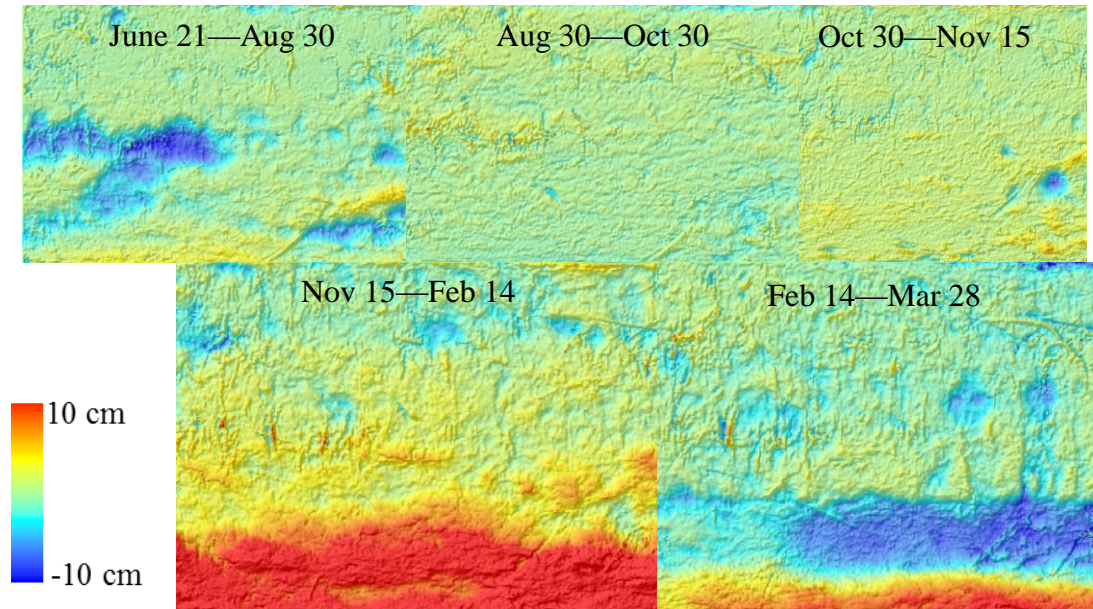
Figure D.4 DoD between the given dates; the color scale is linear from 10 cm (red) to -10 cm (blue). For scale, the width of the Aug 30—Oct 30 figure is ~2 m wide.

Table D.1 RMS error, volume eroded, deposited, net change, and SBR between the given dates

Date	RMS, mm	V_E, L	V_D, L	ΔV	SBR, cm
Jun 21 – Aug 30	2.9	33.70	6.80	-26.90	-0.94
Oct 30 – Nov 15	2.3	4.53	22.37	17.84	0.58
Nov 15 – Feb 14	21	8.78	116.38	107.60	-3.51
Feb 14 – Mar 28	1.0	51.25	22.37	-28.88	-0.99

BIBLIOGRAPHY

Bernhardt, E. S. (2005). Sythesizing U.S. river restoration efforts. *Science*, 308, 636-637.

Brodu, N., & Lague, D. (2012). 3D Terrestrial Lidar data classification of complex natural scenes using a multi-scale dimensionality criterion: applications in geomorphology. *ISPRS Journal of Photogrammetry and Remote Sensing*, 121-134.

Darboux, F., & Huang, C.-h. (2003). An Instantaneous-Profile Laser Scanner to Measure Soil Surface Microtopography. *Soil Science Society of America Journal*, 92-99.

Day, S. S. (2012). *Anthropogenically-Intensified Erosion in Incising River Systems.* Minneapolis: Graduate School of The University of Minnesota.

Entwistle, N. S., & Fuller, I. C. (2009). Terrestrial Laser Scanning to Derive the Surface Grain Size Facies Character of Gravel Bars. In G. L. Heritage, & A. R. Large, *Laser Scanning for the Environmental Sciences* (pp. 102-114). Wiley-Blackwell.

Gilley, J. E., & Kottwitz, E. R. (1995). Random Roughness Assessment by the Pin and Chain Method. *Applied Engineering in Agriculture*, 39-43.

Gosliga, R. v., Lindenbergh, R., & Pfeifer, N. (2006). Derformation Analysis of a Bored Tunnel By Means of Terrestrial Laser Scanning. *Commission V Symposium 'Image Engineering and Vision Metrology'.* Dresden: ISPRS.

Heritage, G., & Large, A. (2009). *Laser Scanning for the Environmental Sciences.* Wiley-Blackwell.

Ho, H.-C., Muste, M., Plenner, S., & Firoozfar, A. (2013). Complementary Experiments for Hydraulic Modeling of Multi-Box Culverts. *Canadian Journal of Civil Engineering*, 324-333.

Hodge, R., Brasington, J., & Richards, K. (2009). In situ characterization of grain-scale fluvial geomorpholgy using Terrestrial Laser Scanning. *Earth Surface Processes and Landforms*, 954-968.

Jester, W., & Klik, A. (2005). Soil Surface Roughness Measurement - Methods, Applicability, and Surface Representation. *Catena*, 174-192.

Lawler, D. M. (1993). The Measurement of River Bank Erosion and Lateral Channel Change: A Review. *Earth Surface Processes and Landforms, 18*, 777-821.

Meral, C. (2011). *Evaluation of Laser Scanning Technology for Bridge Inspection.* Drexel University, Civil Engineering. Philadelphia: Drexel University.

Merrill, S. D., Huang, C., Zobeck, T. M., & Tanaka, D. L. (2001). Use of the Chain Set for Scale-Sensitive and Erosion-Relevant Measurement of Soil Surface Roughness. *E.E. Stott, R.H. Mohtar, G.C. Steinhardt (Eds.), Sustaining the Global Farm 10th International Soil Conservation Organization Meeting Proceedings*, (pp. 594-600). West Lafayette, Indiana.

Moran, M. S. *Army Remote Moisture System.* USDA ARS, Tucson.

Moreno, G. R., Alvarez, D. M., Tarquis, A., Gonzalez, P. A., & Requejo, S. A. (2010). Shadow analysis of soil surface roughness compared to the chain set method and direct measurement of micro-relief. *Biogeosciences*, 7, 2477-2487.

Muste, M. (2009). *Development of Self-Cleaning Culvert Designs.* Iowa Department of Transportation.

Nasermoaddeli, M. H., & Pasche, E. (2008). Application of Terrestrial 3D Laser Scanning in Quantification of the Riverbank Erosion and Deposition. *Riverflow*, (pp. 3-5).

Nettles, C. C. (2010). *Digital Capture of Streambank Erosion Over a Decade Using Terrestrial Laser Scanning, Wilson Creek, Mckinney, Texas (Masters Thesis).* Ann Arbor: ProQuest LLC UMI 1484458.

Nguyen, H., Fernandez-Steeger, T., Wiatr, T., Rodriguez, D., & Azzam, R. (2011). Use of terrestrial laser scanning for engineering geological applications on volcanic rock slpes - an example from Madeira island (Portugal). *Natural Hazards and Earth System Sciences*, 807-817.

Nouwakpo, S., Huang, C.-h., Frankenberger, J., & Bethel, J. (2010). A Simplified Close Range Photogrammetry Method for Soil Erosion Assessment. *2nd Joint Federal Interagency Conference.* Las Vegas.

Odgaard, A. J. (1987). Streambank Erosion Along Two Rivers in Iowa. *Water Resources Research, 23*(7), 1225-1236.

Osterkamp, W. R., Heilman, P., & Lane, L. J. (1998). Economic consideration of a continental sediment-monitoring program. *International Journal of Sediment Resources*, 13(4), 12-24.

Resop, J., & Hession, W. (2010). Terrestrial Laser Scanning for Monitoring Streambank Retreat: Comparison with Traditional Surveying Techniques. *Journal of Hydraulic Engineering*, 794-798.

RUDI. (2014). *3d Modelling Above and Below Ground.* Retrieved from rudi.net: http://www.rudi.net/node/20641

Smith, M., Vericat, D., & Gibbins, C. (2012). Through-Water Terrestrial Laser Scanning of Gravel Beds at the Patch Scale. *Earth Surface Processes and Landforms*, 411-421.

White, L. S., & Cline, J. R. (2009). Interface Software: Point Cloud Registration/Transformation Utility. Dallas: University of Texas.

Zogg, H. M. (2008). *Investigations of High Precision Terrestrial Laser Scanning with Emphasis on the Development of a Robust Close-Range 3D-Laser Scanning System.* Zurich: Institute of Geodesy and Photogrammetry.